Simple Analytical Equations for the Current–Potential Curves at Microelectrodes: A Universal Approach

ARTICLE *in* THE JOURNAL OF PHYSICAL CHEMISTRY C · DECEMBER 2013

Impact Factor: 4.77 · DOI: 10.1021/jp409167m

4 AUTHORS, INCLUDING:

Angela Molina
University of Murcia
210 PUBLICATIONS **1,775** CITATIONS
SEE PROFILE

Joaquín González
University of Murcia
70 PUBLICATIONS **515** CITATIONS
SEE PROFILE

THE JOURNAL OF PHYSICAL CHEMISTRY C

Article

pubs.acs.org/JPCC

Simple Analytical Equations for the Current−Potential Curves at Microelectrodes: A Universal Approach

Angela Molina,*[,†] Joaquin Gonzalez,[†] Edward O. Barnes,[‡] and Richard G. Compton*[,‡]

[†]Departamento de Química Física, Facultad de Química, Regional Campus of International Excellence "Campus Mare Nostrum", Universidad de Murcia, 30100 Murcia, Spain

[‡]Department of Chemistry, Physical and Theoretical Chemistry Laboratory, Oxford University, South Parks Road, Oxford OX1 3QZ, United Kingdom

ABSTRACT: A general, simple, analytical expression for the steady state voltammetric response at electrodes of three different geometries is developed. These geometries have both uniform (isolated microsphere) and nonuniform (microdisc and microsphere supported on an electroinactive surface) accessibility. The expression is applicable over the full range of electrochemical reversibility and for any initial concentrations of both species in the redox couple of interest. By making the assumption that, in all cases, the concentration of each species across the electrode surface is constant (representing an average of the true concentration profile), an equation describing the steady state voltammetric wave is deduced. Although approximate, the developed equation has a high degree of accuracy when compared to simulated results. This method, based on sound physical principles, is open to extension to other geometries and represents an advantage of previous solutions largely restricted to microdiscs.

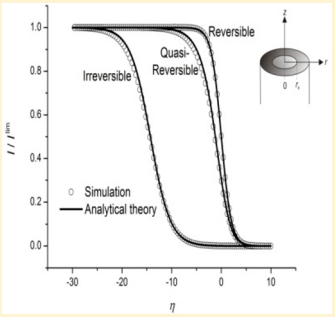

INTRODUCTION

Among the various geometries of the microelectrode, discs are the most used in electrochemistry due largely to the ease with which they can be manufactured and cleaned. However, the voltammetric behavior of nanoparticles adhered to a surface has been of increasing interest, particularly those of approximately spherical geometry. These two geometries, microdiscs and microspheres, require sophisticated numerical methods to solve the corresponding two-dimensional mass transport problem with nonuniform flux gradients over the electrode surface.[1−8]

It is well-known that if electrodes of these geometries are employed in micro- or nanoscale dimensions, steady state voltammetry can be measured with ease, as pioneered by Amatore.[3,9] A variety of theoretical approaches have been used to describe these steady state responses, including both simulation and approximate analytical methods. At first sight the theory for steady-state voltammetry appears simple. However, when the electrochemical processes are kinetically irreversible, analytical treatments become very challenging and have hitherto been carried out on a one-by-one basis for each particular electrode geometry of interest.[4,5,7,8,10−13]

In this paper, we analyze the electrochemical response of a quasi-reversible electrode process taking place at uniformly and nonuniformly accessible electrodes. For the uniformly accessible case, an isolated spherical microsphere is considered. For the nonuniformly accessible case, two geometries are considered, a microdisc electrode and a microsphere electrode resting on an electroinactive surface[14] (see Scheme 1). The latter is used as a model for nanoparticles impacting a surface.[15] The general case where both the oxidized and the reduced species of a redox couple are initially present in solution is considered.

Scheme 1. Geometries and Coordinate Systems of (a) an Isolated Microsphere, (b) a Microdisc Embedded in an Insulating Surface, and (c) a Microsphere Resting on a Nonreactive Surface

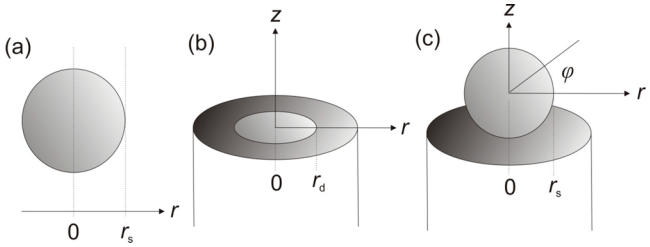

Although approximate, the analytical theory developed here is shown to be a remarkably accurate comparison to simulated results, and previously reported empirical results[5,14] reveals excellent agreement. The equation developed is grounded in plausible physical principles, and is general across all three geometries considered and the full range of electrochemical reversibility, giving it advantages over previous, empirical equation with restricted applicability.

Statement of the Problem. Let us consider the one-electron reduction reaction:

$$O + e^- \underset{k_{ox}}{\overset{k_{red}}{\rightleftarrows}} R \qquad (1)$$

Received: September 13, 2013
Revised: November 11, 2013
Published: December 10, 2013

Table 1. Mass Transport Equations and Boundary Value Problems for the Electrode Geometries Considered[2,3,9]

	SPHERICAL ELECTRODES		DISC ELECTRODE
	Isolated spherical microelectrode	Single conductive spherical electrode	
Mass transport equation	$\frac{\partial c_O}{\partial t} = D\left(\frac{\partial^2 c_O}{\partial r^2} + \frac{2}{r}\frac{\partial c_O}{\partial r}\right)$ $\frac{\partial c_R}{\partial t} = D\left(\frac{\partial^2 c_R}{\partial r^2} + \frac{2}{r}\frac{\partial c_R}{\partial r}\right)$	$\frac{\partial c_O}{\partial t} = D\left(\frac{\partial^2 c_O}{\partial r^2} + \frac{1}{r}\frac{\partial c_O}{\partial r} + \frac{\partial^2 c_O}{\partial z^2}\right)$ $\frac{\partial c_R}{\partial t} = D\left(\frac{\partial^2 c_R}{\partial r^2} + \frac{1}{r}\frac{\partial c_R}{\partial r} + \frac{\partial^2 c_R}{\partial z^2}\right)$	
Boundary Value problem	$t \geq 0,\ r \to \infty$ $t = 0,\ r \geq r_s$ $c_O(r,t) = c_O^*,\ c_R(r,t) = c_R^*$ $t > 0,\ r = r_s$: $D\left(\frac{\partial c_O}{\partial r}\right)_{r=r_s} = k_{red}c_O(r_s) - k_{ox}c_R(r_s)$	$t \geq 0,$ any $r,\ z \to \infty$ any $z,\ r \to \infty$ $t = 0,$ any $r,\ z$ $c_O(r,z,t) = c_O^*,\ c_R(r,z,t) = c_R^*$ $t > 0,\ z = 0,\ r \geq r_s$: $D\left(\frac{\partial c_i}{\partial z}\right)_{z=0,r>r_s} = 0$ $t > 0,\ z \geq r_s,\ r = 0$: $D\left(\frac{\partial c_i}{\partial r}\right)_{z>r_s,r=0} = 0$ $\frac{1}{2}D\int_{\varphi=-\pi/2}^{\varphi=\pi/2}\left[\left(\frac{\partial c_O}{\partial z}\right)\sin\varphi + \left(\frac{\partial c_O}{\partial r}\right)\cos\varphi\right]_{surf}\cos\varphi d\varphi =$ $= k_{red}c_O^{surf} - k_{ox}c_R^{surf}$	$t \geq 0,$ any $r,\ z \to \infty$ any $z,\ r \to \infty$ $t = 0,$ any $r,\ z$ $c_O(r,z,t) = c_O^*,\ c_R(r,z,t) = c_R^*$ $t > 0,\ z = 0,\ r \geq r_d$: $D\left(\frac{\partial c_i}{\partial z}\right)_{z=0,r>r_d} = 0$ $2\pi D\int_{r=0}^{r=r_d}\left(\frac{\partial c_O}{\partial z}\right)_{z=0} r dr = k_{red}c_O(r \leq r_d, z=0) -$ $-k_{ox}c_R(r \leq r_d, z=0)$

where k_{red} and k_{ox} are the heterogeneous rate constants for the electro-reduction and electro-oxidation processes. The particular form of k_{red} and k_{ox} depends on the electrode kinetic model chosen. The above process will be analyzed by assuming that the diffusion coefficients of species O and R are equal and that a large excess of supporting electrolyte is present in the solution in such a way that migration can be neglected.

When the boundary values of the concentrations of electroactive species at the electrode surface and in the bulk are constant, the solution for the diffusion equation at any electrode geometry can be written as[6,7]

$$c_i(q, t) = c_i^* + (c_i^{surf} - c_i^*)f(q, t) i = O, R \quad (2)$$

where q denotes the required coordinates for the electrode geometry considered and c_i^{surf} and c_i^* are the constant values of the concentration of species i at the electrode surface and at the bulk, respectively. $f(q,t)$ is a continuous function dependent on the particular electrode geometry and on time, t.

It is clear that eq 2 can be rigorously applied in the study of a charge transfer process under transient conditions provided that the charge transfer is reversible and the diffusion coefficients of species O and R are equal.[16,17] When either of the assumptions is not fulfilled (for non-reversible electrode processes or non-equal diffusion coefficients), eq 2 is not strictly valid since in this case c_i^{surf} depends on time (except for the case of planar diffusion for which, under reversible conditions, the surface concentrations remain independent of time, even if diffusion coefficients are different).

As the electrode size diminishes, the electrochemical response of the system tends to become stationary or quasi-stationary such that both the average surface concentrations of electroactive species and the average normal surface gradient become independent of time even for nonreversible electrode processes. Under these conditions, eq 2 may be again applicable. This is of great interest since, on the basis of this reasoning, it is possible to obtain general, albeit approximate, simple analytical solutions for microelectrodes of different geometries when the steady state is reached.

In this paper we will analyze the electrochemical response of a quasi-reversible electrode process taking place at spherical or disc electrodes. Spherical electrodes will comprise two different situations: the simplest one corresponding to an isolated spherical microelectrode and the other of a single conductive spherical electrode (or particle) on an infinite electroinactive supporting surface[4,7,14] (see Scheme 1). We will assume that both oxidized and reduced species are initially present in the electrolyte solution.

Thus, the mass transport of the different species in solution and the associated boundary value problems for spherical and disc electrodes is given in Table 1.

Under the above conditions it can be easily deduced that the sum of concentrations of both electroactive species remains constant, regardless of the extent of reversibility of the electrode reaction,[17] that is,

$$c_O(q, t) + c_R(q, t) = c_O^* + c_R^* \quad \forall\ q, t \quad (3)$$

with $q = r$ for isolated spherical electrodes and $q = r, z$ for single conductive spherical and disc electrodes. Symbols are defined in Table 2.

The expression for the current for an isolated spherical electrode or microelectrode (which presents a uniform accessible surface), is the following:

$$I^{sph} = FA^{sph}D\left(\frac{\partial c_O}{\partial r}\right)_{r=r_s} \quad (4)$$

dx.doi.org/10.1021/jp409167m | J. Phys. Chem. C 2014, 118, 346−356

Table 2. Symbols Used

symbol	definition	units
α	transfer coefficient	unitless
c_i	concentration of species i	mol m^{-3}
c_i^*	bulk concentration of species i	mol m^{-3}
c_i^{surf}	surface concentration of species i	mol m^{-3}
D_i	diffusion coefficient of species i	m^2 s^{-1}
E	applied potential	V
E_f^0	formal potential	V
F	Faraday constant (=96485)	C mol^{-1}
I	current	A
J	flux density	mol m^{-2} s^{-1}
k^0	electrochemical rate constant	m s^{-1}
υ	scan rate	V s^{-1}
R	gas constant (=8.314)	J K^{-1} mol^{-1}
r	radial coordinate	m
r_e	disc/sphere radius (e = d or s, respectively)	m
T	temperature	K
t	time	s
z	Z coordinate	m

where "sph" superscript denotes an "isolated spherical electrode". A^{sph} is the area of the spherical electrode ($A^{sph} = 4\pi r_s^2$) and r_s is the sphere radius.

A single conductive spherical electrode on an electroinactive surface and an inlaid disc electrode have nonuniformly accessible surfaces. Therefore, the mass flux density is non uniform and the total flux must be determined by integrating the flux density at each point over the whole surface.

In the case of the single conductive spherical electrode, the mass flux density perpendicular to the surface at any point of the sphere surface is[4,7] (see also Scheme 1)

$$J^{scs} = D\left[\left(\frac{\partial c_O}{\partial z}\right)_{\sqrt{r^2+(z-r_s)^2}=r_s} \sin\varphi + \left(\frac{\partial c_O}{\partial r}\right)_{\sqrt{r^2+(z-r_s)^2}=r_s} \cos\varphi\right] \tag{5}$$

where "scs" superscript denotes a "single conductive sphere" and φ is the angle shown in Scheme 1 (not a spatial coordinate, but an angle useful for current calculations, see ref 10). The average current is obtained by integrating J^{scs} over the electrode surface. So,

$$\frac{I^{scs}}{F} = 2\pi r_s^2 D \int_{\varphi=-\pi/2}^{\varphi=\pi/2}\left[\left(\frac{\partial c_O}{\partial z}\right)_{\sqrt{r^2+(z-r_s)^2}=r_s} \sin\varphi + \left(\frac{\partial c_O}{\partial r}\right)_{\sqrt{r^2+(z-r_s)^2}=r_s} \cos\varphi\right]\cos\varphi \mathrm{d}\varphi \tag{6}$$

For an inlaid disc electrode, the concentration flux density at any point of the disc surface is

$$J^{disc} = D\left(\frac{\partial c_O}{\partial z}\right)_{z=0} \tag{7}$$

and the current is obtained by integrating J^{disc} over the electrode surface as follows:[1,18]

$$\frac{I^{disc}}{F} = 2\pi D \int_{r=0}^{r=r_d}\left(\frac{\partial c_O}{\partial z}\right)_{z=0} r\mathrm{d}r \tag{8}$$

Solutions under Steady State Conditions. Under steady conditions, that is, $\partial c_O/\partial t = \partial c_R/\partial t = 0$, the following expression is obtained for the concentration profile of species O at a isolated spherical electrode,[16,17]

$$c_O^{sph}(r) = c_O^* + (c_O^{surf} - c_O^*)\frac{r_s}{r} \tag{9}$$

For the case of a single conductive spherical electrode, it will be assumed that the expression of the concentration profile for this axi-symmetric system is[7]

$$c_O^{scs}(r,z) = c_O^* + (\tilde{c}_O^{surf} - c_O^*)F(r,z) \tag{10}$$

For disc electrodes it will be assumed that the stationary concentration profile is given by[6,18]

$$c_O^{disc}(r,z) = c_O^* + (\tilde{c}_O^{surf} - c_O^*)\frac{2}{\pi}\int_0^\infty \frac{\sin(mr)}{m} J_0(mr)e^{-mz}\mathrm{d}m \tag{11}$$

with $J_0(x)$ being the zeroth-order Bessel function.[6]

In the eqs 10 and 11, $\tilde{c}_O^{surf}$ denotes a constant average surface concentration.

By introducing eq 9 into eq 4, the following expression is obtained for an isolated spherical microelectrode:

$$\frac{I^{sph}}{F} = A^{sph}D\frac{c_O^* - c_O^{surf}}{\delta^{sph}} \tag{12}$$

with

$$\delta^{sph} = r_s \tag{13}$$

In the case of a single conductive spherical electrode, by introducing eq 10 into eq 6, the following expression for the average current is obtained:[7,10]

$$\frac{I^{scs}}{F} = A^{sph}D\frac{c_O^* - \tilde{c}_O^{surf}}{\delta^{scs}} \tag{14}$$

with $\tilde{c}_O^{surf}$ being the average surface concentration and

$$\delta^{scs} = \frac{r_s}{\ln 2} \tag{15}$$

And in the case of inlaid disc electrodes, by introducing eq 11 into eq 8 one obtains[18]

$$\frac{I^{disc}}{F} = A^{disc}D\frac{(c_O^* - \tilde{c}_O^{surf})}{\delta^{disc}} \tag{16}$$

with δ^{disc} being

$$\delta^{disc} = r_d\frac{\pi}{4} \tag{17}$$

and r_d being the disc radius.

So, under steady state conditions, the following general expression for the current for any electrode geometry can be written:

$$\frac{I}{FA} = D\frac{(c_O^* - \tilde{c}_O^{surf})}{\delta} = (k_{red} + k_{ox})\tilde{c}_O^{surf} - k_{ox}c^* \tag{18}$$

with $c^* = c_O^* + c_R^*$ and δ given by eqs 13, 15, and 17 for spherical, single conductive spherical, and disc electrodes, respectively.

By operating in eq 18 it is possible to obtain a general expression for the average surface concentration of oxidized species for any of the geometries considered:

$$\tilde{c}_O^{surf} = \frac{c_O^* + \bar{k}_{ox}c^*}{1 + \bar{k}_T} \tag{19}$$

where

$$\bar{k}_T = \bar{k}_{ox} + \bar{k}_{red} \tag{20}$$

dx.doi.org/10.1021/jp409167m | J. Phys. Chem. C 2014, 118, 346−356

$$\left.\begin{aligned}\bar{k}_{ox} &= k_{ox}\frac{\delta}{D}\\ \bar{k}_{red} &= k_{red}\frac{\delta}{D}\end{aligned}\right\} \quad (21)$$

The general expression for the current is given in eq 18. By making $c_O^{surf} = 0$ in this equation, the limiting current is obtained,

$$I_{lim} = FAD\frac{c_O^*}{\delta} \quad (22)$$

So

$$\frac{I}{I_{lim}} = 1 - \frac{\tilde{c}_O^{surf}}{c_O^*} = \frac{\bar{k}_{red} - \bar{k}_{ox}\mu}{1 + \bar{k}_T} \quad (23)$$

with

$$\mu = \frac{c_R^*}{c_O^*} \quad (24)$$

Although the expression for the current (eq 23) is formally identical for any electrode geometry, we will give the particular expression for isolated microspheres, single conductive spherical microelectrodes and microdiscs in order to clearly distinguish the current for each particular microelectrode and for comparison with expressions previously reported. In the following, Butler–Volmer kinetics will be assumed. Thus, the current can be written in the general way:

$$\frac{I}{I_{lim}} = \frac{\bar{k}^0 e^{-\alpha\eta}(1 - \mu e^{\eta})}{1 + \bar{k}^0 e^{-\alpha\eta}(1 + e^{\eta})} \quad (25)$$

with $\eta = (F/RT)(E - E_f^0)$ and

$$\left.\begin{aligned}\bar{k}^0)^{sph} &= \frac{k^0 r_s}{D} \quad (a)\\ I_{lim}^{sph} &= FA^{sph}D\frac{c_O^*}{r_s} \quad (b)\end{aligned}\right\} \text{isolated microspheres} \quad (26)$$

$$\left.\begin{aligned}\bar{k}^0)^{scs} &= \frac{k^0 r_s}{D\ln 2} \quad (a)\\ I_{lim}^{scs} &= FA^{sph}D\frac{c_O^*\ln 2}{r_s} \quad (b)\end{aligned}\right\} \text{single conductive microspheres} \quad (27)$$

$$\left.\begin{aligned}\bar{k}^0)^{disc} &= \frac{k^0 r_d}{D}\frac{\pi}{4} \quad (a)\\ I_{lim}^{disc} &= FA^{disc}D\frac{c_O^*}{r_d}\frac{4}{\pi} \quad (b)\end{aligned}\right\} \text{microdiscs} \quad (28)$$

In the above equations, k^0 and α are the heterogeneous rate constant and the charge transfer coefficient, and E_f^0 is the formal potential of the redox couple.

Limiting Cases. *(a). Reversible Processes.* Under reversible conditions (i.e., $k^0 \to \infty$), eq 25 takes the following simpler expression:[17]

$$\frac{I}{I_{lim}} = \frac{1 - \mu e^{\eta}}{1 + e^{\eta}} \quad (29)$$

with I_{lim} given by eqs (26), (27), and (28) for the three geometries under study.

(b). Totally Irreversible Processes. In this case, the condition $k_{red} \gg k_{ox}$ fulfills for all the potentials in such a way that eq 25 becomes in the simplified general equation,

$$\frac{I}{I_{lim}} = \frac{\bar{k}^0 e^{-\alpha\eta}}{1 + \bar{k}^0 e^{-\alpha\eta}} \quad (30)$$

which can also be written:

$$E = E_f^0 + \frac{RT}{\alpha F}\ln(\bar{k}^0) + \frac{RT}{\alpha F}\ln\left(\frac{I_{lim} - I}{I}\right) \quad (31)$$

with $(\bar{k}^0)$ given by equations 26, 27 or 28

Inlaid Disc Microelectrodes. Comparison with Previous Solutions. The case of inlaid disc microelectrodes is of special interest since they are the most commonly used microelectrodes. In this case, eq 23 takes the following simple form:

$$\frac{I^{disc}}{I_{lim}^{disc}} = \frac{k_{red} - k_{ox}\mu}{\frac{D}{r_d}\frac{4}{\pi} + (k_{red} + k_{ox})} \quad (32)$$

which, by assuming Butler–Volmer kinetics, becomes

$$\frac{I^{disc}}{I_{lim}^{disc}} = \frac{e^{-\alpha\eta}(1 - \mu e^{\eta})}{\frac{D}{k^0 r_d}\frac{4}{\pi} + e^{-\alpha\eta}(1 + e^{\eta})} \quad (33)$$

In the more usual case in which R is not initially present in the electrolytic solution ($\mu = 0$), eq 33 simplifies to

$$\frac{I^{disc}}{I_{lim}^{disc}} = \frac{1}{\frac{D}{k^0 r_d}\frac{4}{\pi}e^{\alpha\eta} + (1 + e^{\eta})} \quad (34)$$

with I_{lim}^{disc} given in eq 28.

Equation 34 for the particular case of totally irreversible processes coincides with eq 38 of ref 13 and eq 44 of ref 11, which were deduced assuming uniform surface concentrations for all potentials.

Hitherto, for quasi-reversible processes, empirical expressions have been obtained for the current as a function of electrode potential. Among them, the most used is Oldham's equation given by[5]

$$\frac{I^{disc}}{I_{lim}^{disc}} = 1/\left\{(1 + e^{\eta})\left[1 + \frac{\pi}{(k^0 r_d/D)(\pi/4)e^{-\alpha\eta}(1 + e^{\eta})} \times \left(\frac{(k^0 r_d/D)(\pi/2)e^{-\alpha\eta}(1 + e^{\eta}) + 3\pi}{(k^0 r_d/D)\pi e^{-\alpha\eta}(1 + e^{\eta}) + 3\pi^2}\right)\right]\right\} \quad (35)$$

This equation is still widely used.[2,19−21] However, eq 34 is an approximate analytical solution of this problem under steady state conditions with a clear physical basis.

Equation 35 can be also written in the following way:

$$\frac{I^{disc}}{I_{lim}^{disc}} = \frac{(k^0 r_d/D)(\pi/4)e^{-\alpha\eta}}{F + (k^0 r_d/D)(\pi/4)e^{-\alpha\eta}} \quad (36)$$

with

$$F = 1 - \frac{1 + e^{\eta}}{(3\pi^2/2)e^{\alpha\eta}/(k^0 r_d/D)(\pi/4) + 2(1 + e^{\eta})} \quad (37)$$

so that eq 36 reduces to eq 34 when the condition $\bar{k}^0)^{disc}e^{\alpha\eta}(1 + e^{\eta}) \ll 1$ is fulfilled.

dx.doi.org/10.1021/jp409167m | J. Phys. Chem. C 2014, 118, 346−356

Comparison with Numerical and Previously Reported Results. To validate the above theory, steady state voltammetric simulations were carried out at both microdisc and sphere on a surface geometries. In this section, the results of these simulations are compared to both the above theory and previously reported analytical results.

Microdisc Electrodes. Simulations were carried out using the microdisc model outlined above. Fully reversible, $\overline{k^0})^{\mathrm{disc}} = 1000\pi/4$, quasi-reversible, $\overline{k^0})^{\mathrm{disc}} = \pi/4$, and fully irreversible, $\overline{k^0})^{\mathrm{disc}} = 0.001\pi/4$, heterogeneous kinetics were considered. In each case, the dimensionless scan rate σ was set at 0.0001, small enough to approximate steady state behavior. σ is defined in Table 3, along with other dimensionless parameters.

Table 3. Dimensionless Parameters[a]

parameter	definition
C_i	c_i/c_O^*
$\overline{k^0})^{\mathrm{disc}}$	$(\pi r_d/4D_O)k^0$
$\overline{k^0})^{\mathrm{scs}}$	$(r_s/D_O \ln(2))k^0$
$\overline{k^0})^{\mathrm{sph}}$	$(r_s/D_O)k^0$
K^0	$(r_e/D_O)k^0$
j	$(r_e/c_O{}^*D_O)J$
η	$(RT/F) \times (E - E_f^0)$
τ	$(D_O/r_e^2)t$
R	r/r_e
σ	$(Fr_e^2/RTD_O)v$
Z	z/r_e

[a]Note that r_e refers to either r_s or r_d as appropriate.

α is set at 0.5. The results were compared to the equation developed using eq 34 and the Oldham eq 35. The results are shown in Figure 1. The errors in the two analytical equations (relative to the simulated results) are shown in Figure 2. It is seen that, for fully reversible kinetics, the equations give almost identical results that are in good agreement with the simulated values. As the kinetics become less reversible, however, the results given by the two equations diverge from each other, with the simulated result lying between them. The maximum error in the Oldham equation is 0.5%, and for eq 34, the maximum error is 3.6%.

Concentration profiles across the electrode surface were also simulated for reversible and irreversible electrode kinetics. The simulated results, along with average values calculated from eq 19, are shown in Figure 3a and b for fully reversible and irreversible kinetics, respectively. It is seen that, for fully reversible kinetics, the surface concentration of the parent species is at a constant value (given by the Nernst equation), and logically, the average concentrations coincide with the simulated constant values. For irreversible processes, however, the surface concentration is no longer constant, but increases toward the electrode edge (due to the more efficient radial diffusion). Therefore, the numerical values only coincide with the average concentrations given by eq 19 for limiting current potentials, for which there is no kinetics influence.

As well as the surface concentration profiles, also of particular interest is the variation in the flux density at the electrode surface as a function of radial coordinate. This is shown in Figure 4 for reversible and irreversible kinetics at various points along the steady state voltammetric wave. It is seen that for both reversible and irreversible kinetics, as expected, the flux density increases toward the edge of the electrode. Figure 4b and d show the flux density profiles at the various points on the wave relative to the limiting current flux density profile for reversible and irreversible kinetics, respectively. It is seen that, for the reversible case, the flux density profiles are all approximately the same shape at all points on the wave and scaled to different values (apart from at the edge of the electrode, where edge effects are caused by the singularity). For irreversible kinetics, however, the flux density profiles at the beginning of the wave are much shallower than those at the top and at steady state.

The final feature to be considered is the half wave potential, $\eta_{1/2}$ (the potential at which, when only oxidized species is

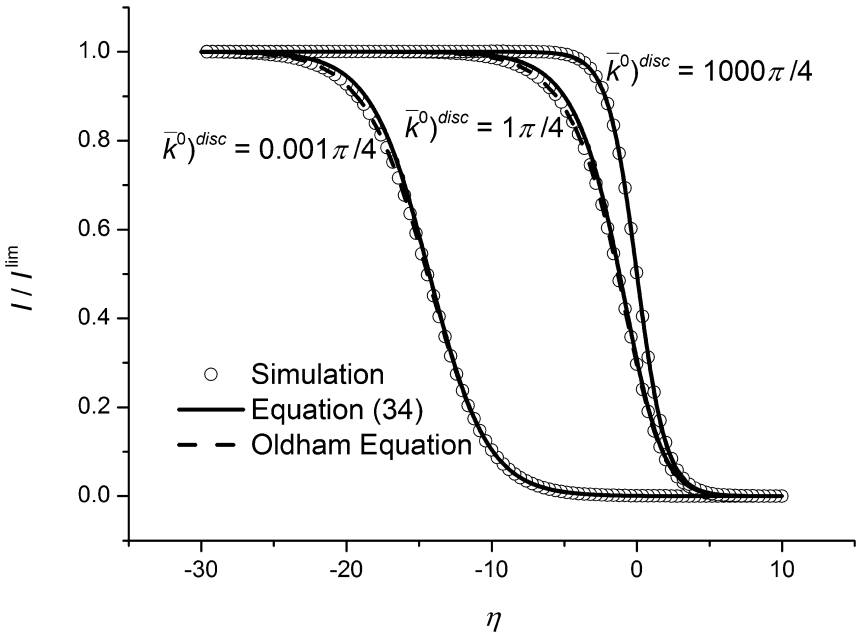

Figure 1. Simulated and analytical steady state voltammograms for the reduction of a single electroactive species at a microdisc electrode for reversible, quasi reversible and irreversible kinetics. In all cases, $\alpha = 0.5$ and $D_O = D_R$.

dx.doi.org/10.1021/jp409167m | J. Phys. Chem. C 2014, 118, 346−356

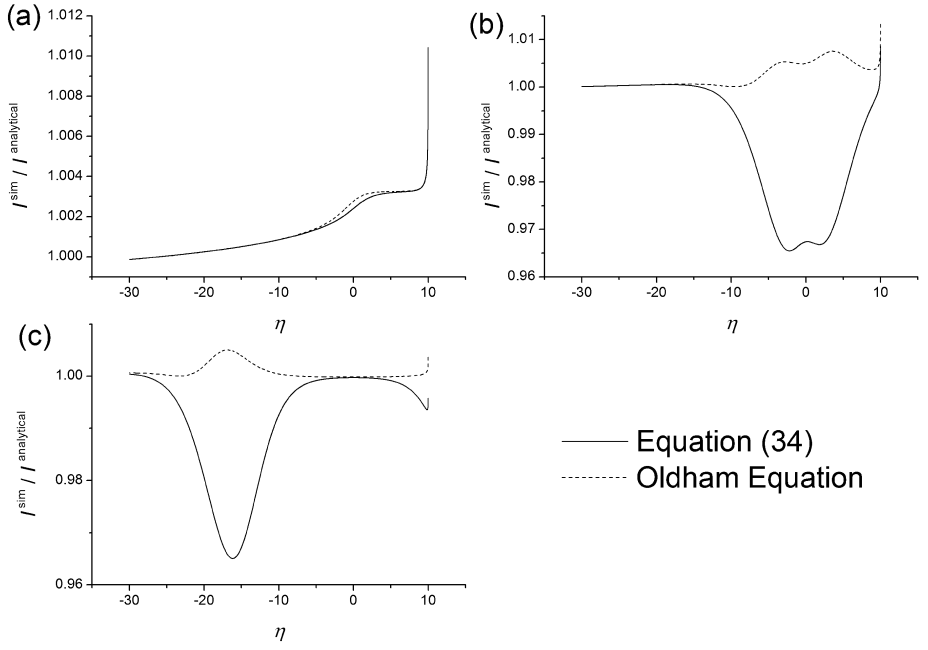

Figure 2. Values of simulated voltammograms relative to eq 35 and the Oldham equation for (a) reversible, $\overline{k}^{0})^{disc} = 1000\pi/4$, (b) quasi-reversible, $\overline{k}^{0})^{disc} = \pi/4$, and (c) irreversible $\overline{k}^{0})^{disc} = 0.001\pi/4$, heterogeneous kinetics.

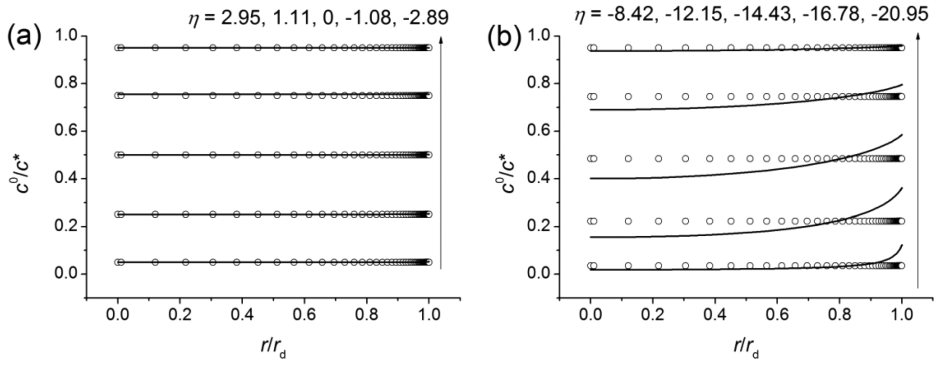

Figure 3. Simulated (lines) and analytical (from eq 19, circles) concentration profiles across the surface of a microdisc electrode for (a) reversible, $\overline{k}^{0})^{disc} = 1000\pi/4$, and (b) irreversible, $\overline{k}^{0})^{disc} = 0.001\pi/4$, heterogeneous kinetics at points on the voltammetric wave corresponding to a current of 5, 25, 50, 75, and 95% of the steady state response. In all cases, $\alpha = 0.5$, and $D_O = D_R$.

initially present, $I = I_{lim}/2$). This was obtained from steady state voltammetric simulations at various values of α and $(\overline{k}^{0})^{disc}$, as well as from eqs 34 and 35. Figure 5a shows the simulated values of $\eta_{1/2}$ against $\log(\overline{k}^{0}))^{disc}$ for α values of 0.7, 0.5, and 0.3. These show the expected linear dependence for low $(\overline{k}^{0})^{disc}$, becoming independent of $((k^0)^{disc})$ at higher values.[10] Figure 5b shows the difference between the $\eta_{1/2}$ values obtained from eq 34 and the simulated values. It is seen that for the most common value of $\alpha = 0.5$, the error is always smaller than 4 mV at 298 K. Figure 5c shows the difference between $\eta_{1/2}$ obtained from the Oldham eq 35 and the simulated value. Here, for $\alpha = 0.5$, the difference is found to be below 1 mV at 298 K. Both equations give a reasonable level of accuracy for $\alpha \geq 0.3$, but the simplistic nature and physical basis of eq 34 gives this an advantage over the Oldham equation.

Sphere on a Surface Electrodes. The only previously reported analytical equation describing the steady state voltammetric response for this geometry is valid only for fully irreversible electrochemical kinetics:[14]

$$\frac{I}{I_{lim}} = \frac{(\overline{k}^{0})^{scs}}{(\overline{k}^{0})^{scs} + e^{\alpha\eta}} \quad (38)$$

which eq 25 is equivalent to in the limit $(\overline{k}^{0})^{scs} \rightarrow 0$. Equation 25, however, is expected to describe the voltammetric waveshape for all values of $(\overline{k}^{0})^{scs}$ This is shown in Figure 6, which shows simulated steady state voltammograms at a sphere on a surface for a variety of $(\overline{k}^{0})^{scs}$ values from fully irreversible to fully reversible. Also shown are analytical results from eq 25. It is seen that eq 25 corresponds closely to the simulated results over the whole range of $(\overline{k}^{0})^{scs}$ values. The value of the simulated steady state voltammograms relative to eq 25 for fully irreversible, quasi-reversible, and fully reversible kinetics is shown in Figure 6. A maximum error of 2.6% is seen (see Figure 7). Equation 26 can therefore be said to accurately produce steady state voltammograms for the sphere on a surface geometry over the full range of electrochemical reversibility.

As with the microdisc geometry, the variation in concentration of electroactive species over the electrode surface was investigated. These were simulated at various points on the

dx.doi.org/10.1021/jp409167m | J. Phys. Chem. C 2014, 118, 346−356

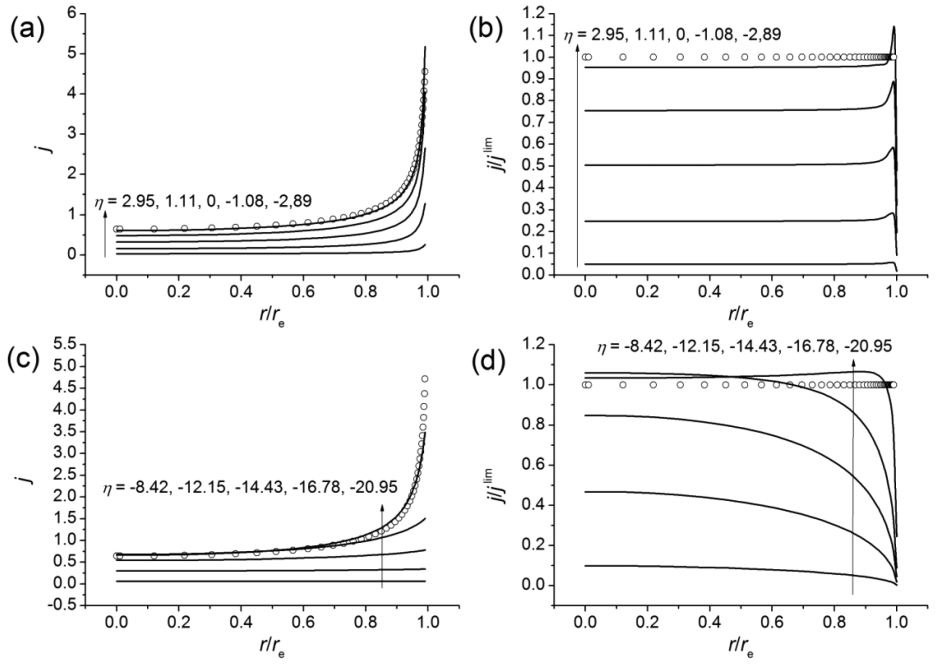

Figure 4. (a) Simulated dimensionless flux density as a function of radial coordinate across a microdisc electrode for a fully reversible process, $(\bar{k}^0)^{disc} = 1000\pi/4$, at points on the voltammetric wave corresponding to 5, 25, 50, 75, and 95% of the steady state response. Circles show the limiting flux density profile (taken at $\eta = -30$). (b) Flux density profiles in (a) shown relative to the limiting flux density profile. (c) As (a) except with $(\bar{k}^0)^{disc} = 0.001\pi/4$ (fully irreversible). (d) As (b) except with $(\bar{k}^0)^{disc} = 0.001\pi/4$. $\alpha = 0.5$.

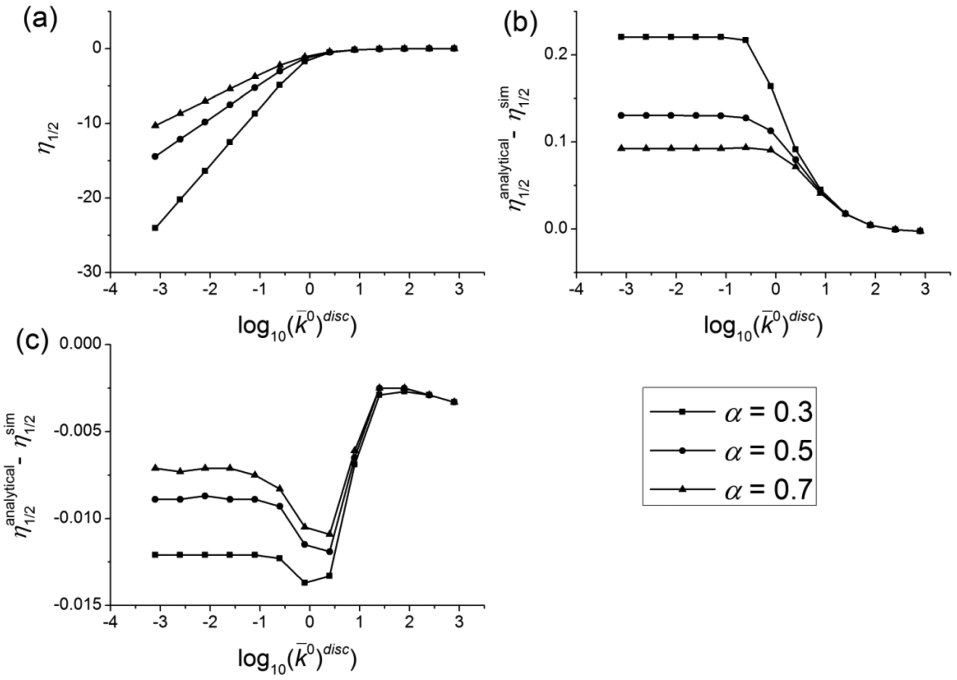

Figure 5. (a) Simulated $\eta_{1/2}$ values for steady state voltammograms at a microdisc with various values of α and $(\bar{k}^0)^{disc}$ (in all cases, $D_O = D_R$). (b) Difference between $\eta_{1/2}$ values calculated using eq 34 and the simulated values. (c) Difference between $\eta_{1/2}$ values calculated using the Oldham eq 36 and the simulated values.

voltammetric waves (at 5, 25, 50, 75, and 95% of the limiting current) for both reversible, $(\bar{k}^0)^{scs} = 1000/\ln(2)$, and irreversible, $(\bar{k}^0)^{scs} = 0.001/\ln(2)$, kinetics. The results, along with average values form eq 19, are shown in Figure 8. As with the microdisc, the fully reversible case (Figure 8a) produced constant surface concentrations given by the Nernst equation, while for irreversible kinetics, nonconstant surface concentrations are observed.

The variation in the flux density at the electrode surface as a function of angular coordinate φ was also studied, for both reversible and irreversible kinetics, at the same points on the voltammograms as in Figure 8. These results are shown

dx.doi.org/10.1021/jp409167m | J. Phys. Chem. C 2014, 118, 346−356

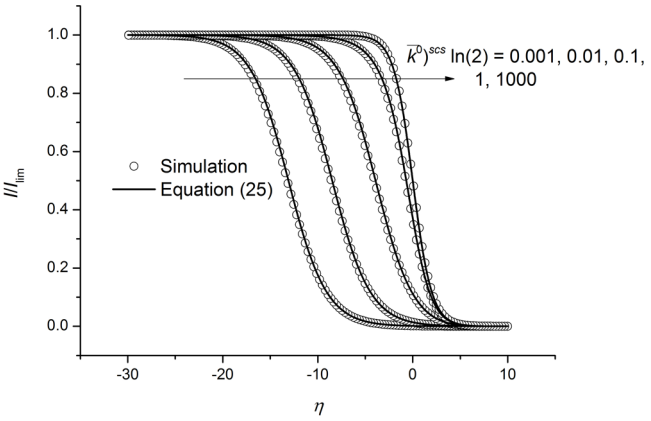

Figure 6. Simulated and analytical steady state voltammograms for the reduction of a single electroactive species at a microsphere electrode on a nonreactive surface for a variety of $(\overline{k}^0)^{scs}$ values. In all cases, α = 0.5, and $D_O = D_R$.

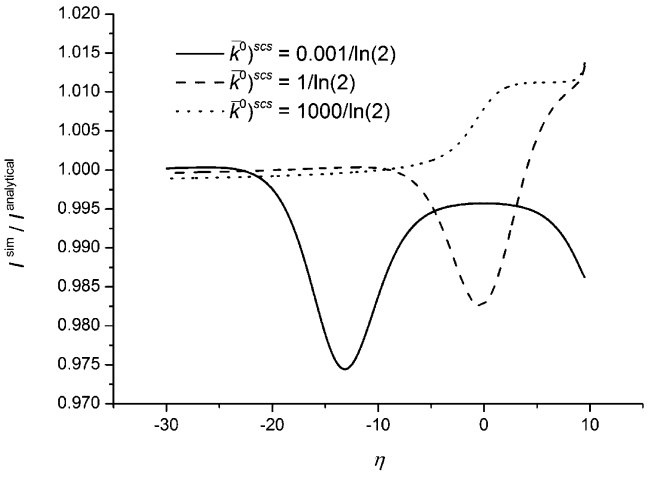

Figure 7. Values of simulated voltammograms relative to eq 25 equation for reversible, quasi reversible and irreversible heterogeneous kinetics at a spherical microelectrode on a non reactive surface. In all cases, α = 0.5 and $D_O = D_R$.

in Figure 9 and are again analogous to the results for the microdisc. As with the microdisc, the flux density profiles in the reversible case are all the same shape (Figure 9a) and differ only in the relative values, which increase the further up the voltammetric wave they are measured. In the irreversible case, however (Figure 9b), the flux density profiles change dramatically in shape at different points on the wave, approaching the limiting steady state value.

As a final validation of eq 25 for the sphere on a surface geometry, dimensionless half wave potentials were obtained from simulations and eq 25 and compared. Figure 10 shows the results, with dimensionless half-wave potentials obtained via simulation shown in Figure 10a, and the difference between those produced via eq 25 and those obtained via simulation shown in Figure 10b, all for various values of $(\overline{k}^0)^{scs}$ and α. As with the microdiscs, the simulations produced values following expected qualitative trends. As in the case of the disc electrode the difference between a simulated and analytical value for α = 0.5 was found to be smaller than 3 mV at 298 K.

The good agreement in waveshapes between simulated results and those produced using the analytical theory outlined above, for both microdiscs and spheres resting on a surface, lends support to eq 25 as a simple approximate equation with a sound physical basis to produce steady state voltammetry at these geometries (in the case of spheres on a surface, for the first time for both irreversible and reversible heterogeneous kinetics). We note that a similar approximation, namely, of using uniformity of accessibility, as been usefully applied in the description of hydrodynamic electrodes such as the channel electrode.[22−24]

CONCLUSIONS

A general analytical expression has been developed for the steady state current voltammetric response for microelectrodes of three different geometries. This expression is applicable for any degree of reversibility of the charge transfer process, and for when both species of the redox couple are initially present in the electrolytic solution in any concentration ratio. From it, limiting cases corresponding to Nernstian and fully irreversible processes have been deduced.

Of particular interest is the application of this simple expression to non uniformly accessible disc electrodes and single spherical electrodes, or nanoparticles, supported on an electroinactive surface. The case of disc microelectrodes is remarkable since they are by far the most popular microelectrodes used and they present serious difficulties for analytically solving the transport to the electrode due to the nonuniform current densities. For both these geometries, good agreement between simulated and theoretical results has been found. The solution

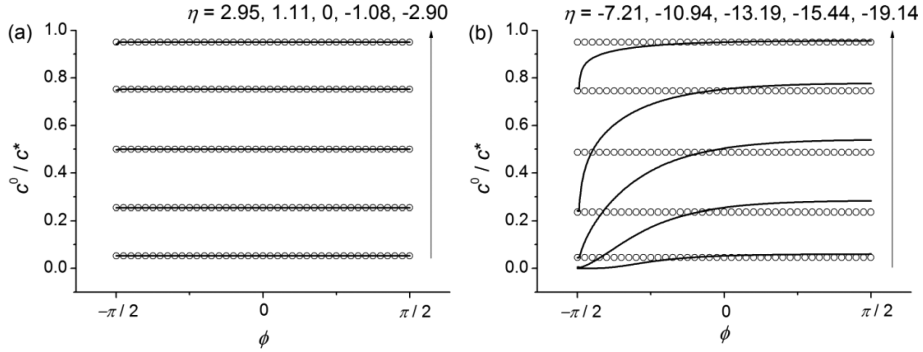

Figure 8. Simulated (lines) and analytical (from eq 19, circles) concentration profiles across the surface of a microsphere electrode on a nonreactive userface for (a) reversible, $(\overline{k}^0)^{scs}$ = 1000/ln(2), and (b) irreversible, $(\overline{k}^0)^{scs}$ = 0.001/ln(2), heterogeneous kinetics at points on the voltammetric wave corresponding to a current of 5, 25, 50, 75, and 95% of the steady state response. In all cases, α = 0.5, and $D_O = D_R$.

dx.doi.org/10.1021/jp409167m | J. Phys. Chem. C 2014, 118, 346−356

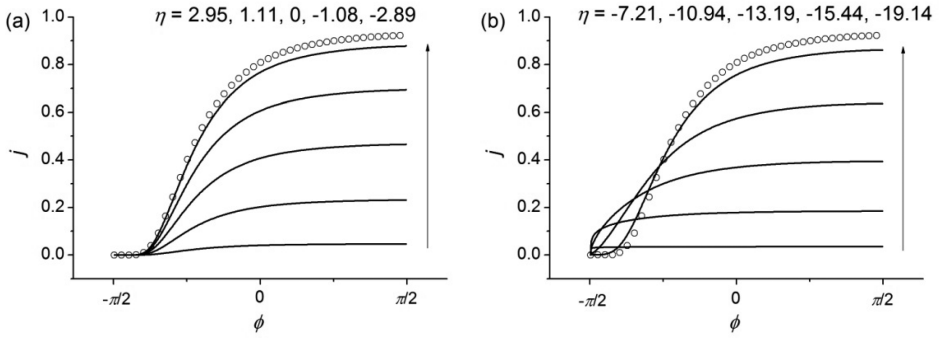

Figure 9. (a) Simulated dimensionless flux density as a function of angular coordinate across a microsphere electrode on a non reactive surface for a fully reversible process, $(\bar{k}^0)^{scs} = 1000/\ln(2)$, at points on the voltammetric wave corresponding to 5, 25, 50, 75, and 95% of the steady state response. Circles show the limiting flux density profile (taken at $\eta = -30$). (b) As (a) except with $(\bar{k}^0)^{scs} = 0.001/\ln(2)$ (fully irreversible). $\alpha = 0.5$.

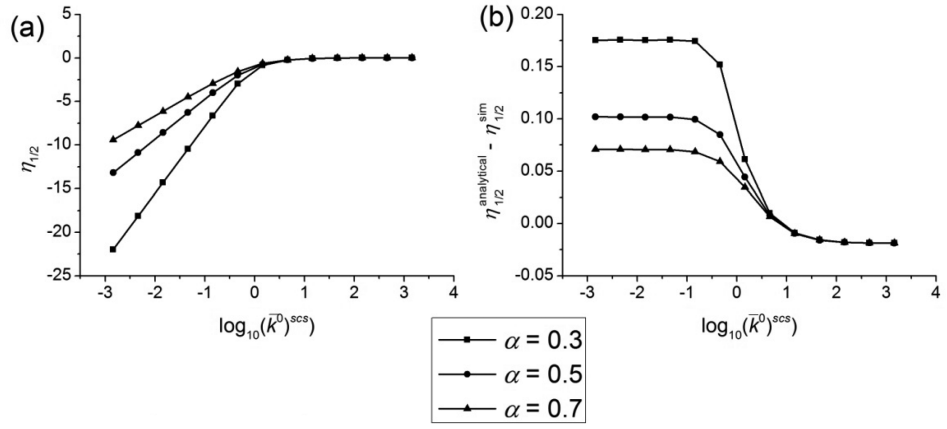

Figure 10. (a) Simulated $\eta_{1/2}$ values for steady state voltammograms at a sphere on a surface with various values of α and $(\bar{k}^0)^{scs}$ (in all cases, $D_O = D_R$). (b) Difference between $\eta_{1/2}$ values calculated using eq 25 and the simulated values.

presented here is based on sound physical principles, and represents a comprehensive strategy to address the study of steady state responses for charge transfer processes at electrodes of any geometry, as opposed to previous approaches mostly restricted to microdisc electrodes.

APPENDIX: SIMULATION METHODS

A simple, one-electron reduction, as given in eq 1, is considered to occur at the surface of a microdisc electrode (shown schematically in Scheme 1b) or a single conductive spherical electrode resting on a non reactive surface (shown schematically in Scheme 1c). A large amount of excess supporting electrolyte is assumed to suppress electric fields and ensure that all diffusion is mass transport only. The mass transport equations and boundary conditions for both geometries are summarized in Table 1 and detailed below.

Linear sweep voltammetry (LSV) is simulated, where the flux density of material (normal to the electrode surface) is described by the Butler–Volmer equation:

$$D\frac{\partial c_i}{\partial N} = k^0[c_O^{surf}\ \exp(-\alpha\eta) - c_R^{surf}\ \exp((1-\alpha)\eta)] \quad (39)$$

where $\eta = F(E - E_f^0)/(RT)$ and N is some coordinate normal to the electrode surface, and all other symbols are defined in Table 2. In the case of a microdisc, N is simply the z coordinate. In the case of a sphere on a surface, the flux density normal to the surface can be split into components in the r and z directions:

$$D\frac{\partial c_i}{\partial r} = k^0[c_O^{surf}\ \exp(-\alpha\eta) - c_R^{surf}\ \exp((1-\alpha)\eta)]\cos\varphi \quad (40)$$

$$D\frac{\partial c_i}{\partial z} = k^0[c_O^{surf}\ \exp(-\alpha\eta) - c_R^{surf}\ \exp((1-\alpha)\eta)]\sin\varphi \quad (41)$$

A series of dimensionless parameters are introduced, which serve to remove scaling factors from the simulations. These are listed in Table 3. Scheme 2 shows the dimensionless simulations spaces used to model both the embedded microdisc and the sphere resting on a surface. Upon introduction of these parameters (and noting that if all diffusion coefficients are considered equal, as is the case throughout this study, then all dimensionless diffusion coefficients are equal to unity and may be neglected) the mass transport equation becomes

$$\frac{\partial C_i}{\partial \tau} = \frac{\partial^2 C_i}{\partial R^2} + \frac{1}{R}\frac{\partial C_i}{\partial R} + \frac{\partial^2 C_i}{\partial Z^2} \quad (42)$$

The Butler–Volmer boundary condition for the electrode surface becomes

$$\frac{\partial C_i}{\partial N} = K^0[C_O^{surf}\ \exp(-\alpha\eta) - C_R^{surf}\ \exp((1-\alpha)\eta)] \quad (43)$$

Note that when carrying out simulations, K^0 is defined in the same way (as shown in Table 3), regardless of geometry. Zero flux boundary conditions are imposed at electroinactive surfaces

dx.doi.org/10.1021/jp409167m | J. Phys. Chem. C 2014, 118, 346–356

Scheme 2. Simulation Spaces (in Dimensionless Coordinates) Used in the Simulation of (a) a Microdisc and (b) a Sphere on a Surface

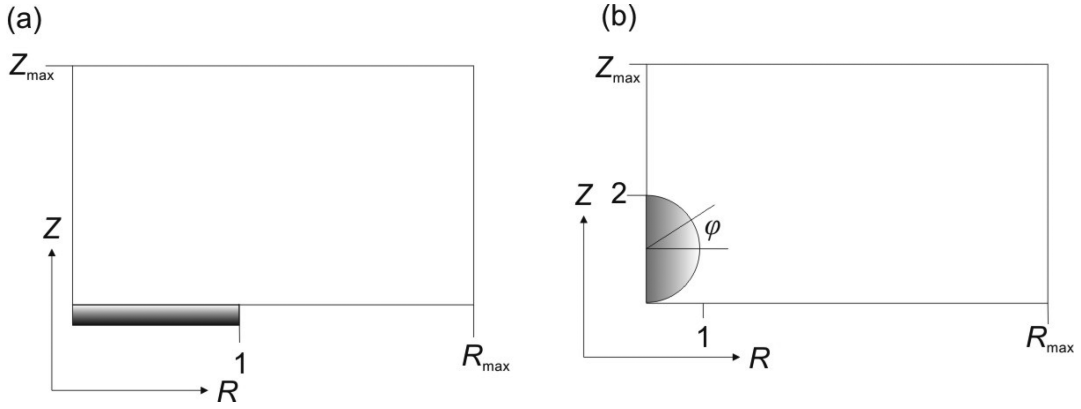

and across the $R = 0$ symmetry axis. Maximum R and Z coordinates are set at

$$R_{max}^{disc} = 1 + 6\sqrt{\tau_{max}} \quad (44)$$

$$R_{max}^{sphere} = 1 + 6\sqrt{\tau_{max}} \quad (45)$$

$$Z_{max}^{disc} = 6\sqrt{\tau_{max}} \quad (46)$$

$$Z_{max}^{sphere} = 2 + 6\sqrt{\tau_{max}} \quad (47)$$

as a distance, $6(\tau_{max})^{1/2}$ has been shown to be well beyond the depletion zone[21] (τ_{max} is the total dimensionless time of the simulated experiment). At these boundaries, all concentrations are set at their bulk values. Initially, we only consider species O to be present in solution at uniform concentration.

In LSV, the dimensionless applied overpotential, η, swept from some starting potential, η_{start} at a dimensionless scan rate of σ units of η per unit τ, to some ending potential. For a reduction, this is described mathematically as:

$$\eta = \eta_{start} - \sigma\tau \quad (48)$$

To calculate the total dimensionless current at any given time, the (dimensionless) flux density, j (defined in Table 3), must be integrated over the whole electrode. For the disc electrode, this is given by the expression

$$j^{disc} = \int_0^1 \left(\frac{\partial C_O}{\partial Z}\right)_{Z=0} R\,dR \quad (49)$$

and for a sphere by

$$j^{scs} = \int_{\varphi=-\pi/2}^{\varphi=\pi/2} \left[\left(\frac{\partial C_O}{\partial Z}\right)_{R^2+(Z-1)^2=1} \sin\varphi + \left(\frac{\partial C_O}{\partial R}\right)_{R^2+(Z-1)^2=1} \cos\varphi\right] \cos\varphi\, d\varphi \quad (50)$$

with

$$\frac{I}{I_{lim}} = \frac{j}{j_{lim}} \quad (51)$$

Computational Methods

The alternating direction implicit (ADI) method[26] was used to discretise the mass transport equation and boundary conditions for numerical solution. The spatial grid the equations were solved over differs for the two geometries. For the sphere on a surface, N_s spatial points were spaced evenly around the surface of the sphere (defined as the continuous line satisfying the equation $R^2 + (Z - 1)^2 = 1$). The coordinates of these points then act to define the R grid for $R \leq 1$ and the Z grid for $Z \leq 2$. Beyond this, the grid expands in both directions according to:

$$Q_{j+1} = Q_j + \gamma(Q_j - Q_{j-1}) \quad (52)$$

where Q_j is the jth R or Z grid point.

For the microdisc simulations, an initial step size of Δ is defined for the first step in the Z grid, and the first steps in either direction from the predefined point of $R = 1$ (the electrode edge) in the R grid. Both grids then expand in the same manner as for the sphere on a surface to the edges of the simulation space.

For both geometries, the temporal grid is defined by dividing each unit of η into N_η equally spaced points. Convergence studies were carried out and it was found the following parameters produced results within 0.2% of a fully converged result: $N_s = 400$, $\gamma = 1.25$, $\Delta = 8 \times 10^{-5}$, and $N_\eta = 10000$.

The discretized equations were solved simultaneously, with the Thomas Algorithm[27] being used to solve the large banded matrices. Simulations were coded in C++ and run on an Intel(R) Xeon(R) 2.26 GHz PC with 2.25 GB RAM, with a typical run time of 20 minutes.

AUTHOR INFORMATION

Corresponding Author

*E-mail: amolina@um.es; richard.compton@chem.ox.ac.uk.

Notes

The authors declare no competing financial interest.

ACKNOWLEDGMENTS

The authors greatly appreciate the financial support provided by the Ministerio de Economia y Competitividad (Project Number CTQ2012-36700, cofunded by European Regional Development Fund), the Fundación SENECA de la Región de Murcia (Project Number 08813/PI/08), and St John's College, Oxford.

REFERENCES

(1) Henstridge, M. C.; Compton, R. G. Mass Transport to Micro- and Nanoelectrodes and Their Arrays: a Review. *Chem. Rec.* **2012**, *12*, 63−71.

(2) Compton, R. G.; Banks, C. E. *Understanding Voltammetry*, 2nd ed.; World Scientific: Oxford, 2012.
(3) Amatore, C. In *Physical Electrochemistry: Principles, Methods and Applications*; Rubinstein, I., Ed.; Marcel Dekker: New York, 1995; Chapter 4.
(4) Streeter, I.; Compton, R. G. Diffusion-Limited Currents to Nanoparticles of Various Shapes Supported on an Electrode: Spheres, Hemispheres, and Distorted Spheres and Hemispheres. *J. Phys. Chem. C* **2007**, *111*, 18049−18054.
(5) Oldham, K. B.; Zoski, C. G. Steady-State Voltammetry at an Inlaid Microdisc: Comparison of Three Approaches. *J. Electroanal. Chem.* **1991**, *313*, 17−28.
(6) Crank, J. *The Mathematics of Diffusion*, 2nd ed.; Oxford Science Publications: U.K., 1980.
(7) Bobbert, P. A.; Wind, M. M.; Vlieger, J. Diffusion to a Slowly Growing Truncated Sphere on a Substrate. *Phys. A* **1987**, *141*, 58−72.
(8) Molina, A.; Gonzalez, J.; Henstridge, M. C.; Compton, R. G. Analytical Expressions for Transient Diffusion Layer Thicknesses at Non Uniformly Accessible Electrodes. *Electrochim. Acta* **2011**, *56*, 4589−4594.
(9) Klymenko, O. V.; Svir, I.; Oleinick, A.; Amatore, C. A Novel Approach to the Simulation of Electrochemical Mechanisms Involving Acute Reaction Fronts at Disk and Band Microelectrodes. *ChemPhysChem* **2012**, *13*, 845−859.
(10) Phillips, C. G. The Steady-State Current for a Microelectrode near Diffusion-Limited Conditions. *J. Electroanal. Chem.* **1990**, *291*, 251−256.
(11) Xiaoping, L.; Juntao, L.; Chuansin, Ch. The General Characteristics of Microelectrodes of Any Planar Geometry under Steady State Conditions. *J. Electroanal. Chem.* **1990**, *295*, 15−23.
(12) Oldham, K. B. Steady-State Voltammetry at Microelectrodes of Arbitrary Geometry. *J. Electroanal. Chem.* **1992**, *323*, 53−76.
(13) Streeter, I.; Compton, R. G. Steady State Voltammetry at Non-Uniformly Accessible Electrodes: A Study of Tafel Plots for Microdisc and Tubular Flow Electrodes in the Reversible and Irreversible Limits of Electron Transfer. *Phys. Chem. Chem. Phys.* **2007**, *9*, 862−870.
(14) Ward, K. R.; Lawrence, N. S.; Hartshorne, R. S.; Compton, R. G. Modelling the Steady State Voltammetry of a Single Spherical Nanoparticle on a Surface. *J. Electroanal. Chem.* **2012**, *683*, 37−42.
(15) Kahk, J. M.; Rees, N. V.; Pillay, J.; Tshikhudo, R.; Vilakazi, S.; Compton, R. G. Electron Transfer Kinetics at Single Nanoparticles. *Nano Today* **2012**, *7*, 174−179.
(16) Molina, A.; Serna, C.; Camacho, L. Conditions of Applicability of the Superposition Principle in Potential Multipulse Techniques: Implications in the Study of Microelectrodes. *J. Electroanal. Chem.* **1995**, *394*, 1−6.
(17) Molina, A.; Gonzalez, J.; Henstridge, M.; Compton, R. G. Voltammetry of Electrochemically Reversible Systems at Electrodes of Any Geometry: A General, Explicit Analytical Characterization. *J. Phys. Chem. C* **2011**, *115*, 4054−4062.
(18) Saito, Y. A Theoretical Study on the Diffusion Current at the Stationary Electrodes of Circular and Narrow Band Types. *Rev. Polarograph.* **1968**, *15*, 177−187.
(19) Bard, A. J.; Mirkin, M. V *Scanning Electrochemical Microscopy*, 2nd ed.; CRC Press: New York, 2012.
(20) Wang, Y.; Velmurugan, J.; Mirkin, M. V. Kinetics of Charge-Transfer Reactions at Nanoscopic Electrochemical Interfaces. *Isr. J. Chem.* **2010**, *50*, 291−305.
(21) Molina, A.; Gonzalez, J. In *Characterization of Materials*, 2nd ed.; Kaufman, E. N., Ed.; Wiley: New York, 2012.
(22) Compton, R. G.; Pilkington, M. B. G.; Stearn, G. M.; Unwin, P. R. Mass-Transport to Channel and Tubular Electrodes - The Singh and Dutt Approximation. *J. Electroanal. Chem.* **1987**, *238*, 43−66.
(23) Unwin, P. R.; Compton, R. G. The Relationship Between Mass-Transport to Channel and Rotating-Disk Electrodes. *J. Electroanal. Chem.* **1988**, *245*, 287−298.
(24) Compton, R. G.; Unwin, P. R. A Critical-Assessment of the Theories for Linear Sweep Voltammetry of Reversible Electrode Processes at a Channel Electrode. *J. Electroanal. Chem.* **1989**, *264*, 27−36.
(25) Einstein, A. On the Movement of Small Particles Suspended in Stationary Liquids Required by the Molecular-Theory of Heat. *Ann. Phys.* **1905**, *17*, 549−560.
(26) Britz, D. *Digital Simulation in Electrochemistry*, 3rd ed.; Springer: Heidelberg, Germany, 2005.
(27) Press, W. H.; Teukolsky, S. A.; Vetterling, W. T.; Flannery, B. P. *Numerical Recipes*, 3rd ed.; Cambridge University Press: Cambridge, 2007.